Journal of Computational Physics 228 (2009) 3464–3477

Contents lists available at ScienceDirect

Journal of Computational Physics

journal homepage: www.elsevier.com/locate/jcp

Compressive sensing for multi-static scattering analysis

Lawrence Carin *, Dehong Liu, Wenbin Lin, Bin Guo

Department of Electrical and Computer Engineering, Duke University, Durham, NC 27708-0291, United States

ARTICLE INFO

Article history:
Received 23 May 2008
Received in revised form 18 December 2008
Accepted 27 January 2009
Available online 7 February 2009

Keywords:
Compressive sensing
Scattering
Numerical

ABSTRACT

Compressive sensing (CS) is a framework in which one attempts to measure a signal in a compressive mode, implying that fewer total measurements are required *vis à vis* direct sampling methods. Compressive sensing exploits the fact that the signal of interest is compressible in some basis, and the CS measurements correspond to projections (typically random projections) performed on the basis function coefficients. In this paper, we demonstrate that ideas from compressive sensing may be exploited in the context of electromagnetic modeling, here multi-static scattering from an arbitrary target. In this context, the computational analysis may be viewed as a numerical experiment, and ideas from compressive sensing may be used to reduce the number of computations required for target characterization. It is demonstrated that the compressive sensing framework may be applied with relatively minor modifications to many existing numerical models, with examples presented here for a fast-multipole computational engine.

1. Introduction

In the 1990s there were significant developments on the sparse representation of digital signals in terms of orthonormal basis functions. For example, assume that one is interested in representing the m-dimensional complex signal u in terms of a basis, of the form $u = \Psi\theta$, where Ψ is an $m \times m$ matrix and θ represents an m-dimensional column vector; the columns of Ψ represent the m orthonormal basis vectors. For most natural signals u (characterized by being piecewise smooth), the wavelet transform [1,2] has been shown to yield a particularly sparse representation. Specifically, if θ represents the wavelet coefficients for a piecewise smooth signal u, then the error $\|\theta - \theta_N\|_2^2$ has been shown to decay quickly with increasing N, where θ_N represents θ with the smallest $m - N$ coefficients set to zero. This implies that only a small number N of dominant wavelet coefficients are required to approximate u well. This property of wavelets has led to a new generation of wavelet-based compression algorithms, for both imagery and video [3,4]. Importantly, since the N dominant wavelet coefficients are a strong function of the signal u of interest, the aforementioned compression algorithms must adapt to u. In addition, we note that the discrete cosine transform (DCT) is at the heart of JPEG compression [5], which is currently the industry compression standard; this is because most images (and video) are highly compressible in a DCT basis.

While wavelet and DCT-based compression and sparse signal representations have had many important practical applications, in the context of sensing there are issues worthy of further research. For example, in the above discussion it was noted that for a compressing basis the $m - N$ smallest transform coefficients may be discarded with minimal degradation to the reconstruction of u (*i.e.*, $\|\theta - \theta_N\|_2^2$ decreases quickly as N increases). However, in the context of sensing, one must first measure the m-dimensional digital signal u, represent it in the basis Ψ, and then compression is performed subsequently, after which effectively θ_N is retained. Consequently, in some sense $m - N$ pieces of data in the original u were measured

* Corresponding author. Tel.: +1 919 660 5270; fax: +1 919 660 5293.
E-mail addresses: lcarin@ece.duke.edu (L. Carin), liudh@ece.duke.edu (D. Liu), wl@ece.duke.edu (W. Lin), bg25@ece.duke.edu (B. Guo).

0021-9991/$ - see front matter © 2009 Elsevier Inc. All rights reserved.
doi:10.1016/j.jcp.2009.01.033

unnecessarily. Compressive sensing (CS)[1] [6–8] is a new approach to data collection, seeking to integrate sensing and compression and therefore measure the informative part of the signal directly. The above discussion was placed in the context of wavelets and the DCT, while CS is applicable to any basis or frame Ψ in which the signal of interest u may be sparsely rendered [6–8].

There are several "surprising" aspects of compressive sensing [8]. First, in the above discussion it was noted that the largest N coefficients θ_N are a strong function of the signal u, and the approximation to u based on θ_N yields a good representation with $N \ll m$. Therefore, one may anticipate that the CS measurements should be performed adaptively, with the system "homing in" in some sense on the dominant coefficients θ_N. A surprising aspect of CS is that one does not attempt to measure the dominant coefficients θ_N; rather, a weighted combination of *all* transform coefficients θ are measured. Another surprising aspect of CS is that one may expect that the aforementioned weights should adapt to the signal under test; however, CS theory indicates that a fixed set of weights may be used for all u within a given class, and that the quality of the CS estimate of u, based on these measurements, will not be significantly worse than the best adaptive measurements. A set of n CS measurements may be represented as $v = \Phi\theta$, where Φ is an $n \times m$ projection matrix. One additional "surprise" is that the components of Φ may be constituted as draws from a general underlying random variable. Summarizing, (i) in CS measurements one does not directly measure u, but measures u (or, equivalently, θ) projected onto a random signal, and n such random projections constitute the n-dimensional CS measurement vector v; (ii) the particular n projection vectors may be constituted randomly, and are fixed for all u; (iii) one may use CS inversion techniques to approximate u accurately based on the measurements v, with several techniques available for this inversion [9–11,7,12–14].

In this paper, we address the concept of using compressive sensing for numerical electromagnetic scattering computations. When performing such a scattering analysis, one typically must solve a complex matrix equation of the form $Zi = e$, where Z may represent an "impedance" matrix, i is a column vector of induced currents, and e is a column vector representing the excitation (for example, any algorithm in the general form of the method of moments [15] falls into this category, with the recently developed fast-multipole method constituting an important modern example [16–18]). Assume that one is interested in performing a multi-static scattering analysis at a fixed frequency, as a function of the incidence and scattering angles (*e.g*, in two dimensions, with the signal of interest u being the scattered fields as a function of angles ϕ_i and ϕ_s). When considering plane wave excitation, each incident angle ϕ_i corresponds to a distinct e, and the associated computed induced current i is then used to compute the scattered fields [15] at all angles ϕ_s. In almost all previous analyses researchers have considered excitations e corresponding to a plane wave, and for each such excitation the computed i is then employed to compute the scattered fields individually at all angles ϕ_s.

As indicated above, the data u of interest is the complex "image" of multi-static scattered fields, with two axes corresponding to ϕ_i and ϕ_s (for a fixed frequency). The computation of u for a given target is often a computationally challenging task, particularly as the target increases in size relative to wavelength (this problem having motivated the work in [16–18], as well as other "fast" computational engines). The challenge is that when plane wave excitation is considered, the number of different incident angles ϕ_i that must be considered is relatively large, and for each there is a need to constitute and solve a large matrix equation $Zi = e$. As discussed further below, and as required for a compressive sensing analysis, a multi-static scattering image such as u is typically highly compressible within an appropriate orthonormal basis Ψ (*e.g.* the DCT). Based on this, one may view the computation of u as a *computational* sensing challenge, for a target of interest. Rather than applying compressive sensing to a physical sensing challenge, we will here apply it to a numerical sensing problem (computation of multi-static scattered fields). Specifically, rather than considering one set of excitation and scattering angles at a time, we will consider a linear combination of *all* excitation and scattering angles *simultaneously*. The linear weights will be constituted as draws from a random process. We will demonstrate that this compressive sensing form of electromagnetic scattering computations may be implemented with minor modification to existing computational engines (*e.g.* [16–18]), while providing computational acceleration (fewer total computations required to attain the same scattering data). In this manner, the numerical model is used to directly compute the compressive data v, and then CS inversion [9–11,7,12–14], is employed to recover the desired data u.

The remainder of the paper is organized as follows. In Section 2, we provide a concise summary of compressive sensing theory, and in Section 3 we demonstrate how complex scattering physics may be employed to achieve projection-based measurements that are appropriate for CS. In Section 4, we consider a very practical application, with these ideas used as a tool for accelerating numerical multi-static scattering analyses. Example scattering results using compressive sensing applied to fast-multipole [16–18] analyses are presented in Section 5. Conclusions of this work are discussed in Section 6.

2. Review of compressive sensing theory

The field of compressive sensing was started by Candès et al. [7] by considering signals that are sparse in the Fourier domain, with this generalized subsequently by Candès and Tao [19] to signals that are sparse in general bases or frames. Donoho [8] developed further results along these lines. In the wave problem of interest here, we will be considering complex signals u. The first paper in this field [7] considered complex signals, while [20] considered real signals and possibly complex projections. Other papers in this field [8,19] have focused exclusively on real signals. However, it is noted in [19] that the

[1] All compressive sensing preprints in the list of references may be downloaded from http://www.dsp.ece.rice.edu/cs/.

theory extends directly to complex signals, except for negligible changes to some of the constants in the performance analyses. Consequently, in the discussion that follows we consider compressive sensing in the context of complex signals u.

2.1. Sparsity

In the discussion below we adopt notation introduced by Donoho [8]. Consider a class U of m-dimensional complex signals. An information operator I_n maps any member of U to an n-dimensional complex vector, $I_n : U \rightarrow \mathbf{C}^n$. The information operator is of the form

$$I_n(u) = (\langle \xi_1, u\rangle, \ldots, \langle \xi_n, u\rangle), \tag{1}$$

where $\langle \xi_i, u\rangle$ is an inner product and ξ_i are sampling vectors ($\langle \xi_i, u\rangle = \xi_i^H u$, where superscript H represents the complex transpose). We let A_n represent an algorithm that operates on the n-dimensional signal measured by the information operator I_n, and A_n attempts to reconstruct $u, A_n : \mathbf{C}^n \rightarrow \mathbf{C}^m$; the characteristics of such an algorithm are discussed below.

If the m-dimensional signals in U have special properties, u may be recovered accurately even when the number of measurements $n \ll m$, this yielding the terminology "compressive sensing". The exploitation of known constraints on the properties of signals in U may be viewed as a regularization of the mapping $A_n : \mathbf{C}^n \rightarrow \mathbf{C}^m$. In compressive sensing (CS) one exploits the fact that most natural signals u are compressible in an appropriate orthonormal basis, for example a wavelet [1,2], local Fourier [2], or DCT [5] basis. The original goal of CS was to directly measure the informative part of the signal u, such that the total number of samples that must be measured may be reduced substantially, potentially simplifying the hardware properties of the sensor digitization system. In this context, the measurements are themselves directly performed in a compressive mode. In this paper we extend these ideas to reduce the number of computations required for a numerical multi-static scattering analysis.

Focusing now on sparsity, let $\{\psi_i\}_{i=1,m}$ represent an orthonormal basis for m-dimensional signals, and therefore for $u \in U$ we have $u = \sum_{i=1}^m \theta_i \psi_i$, with $\theta_i \equiv \langle u, \psi_i\rangle$. The set U is termed compressible if for all $u \in U$

$$\|\theta\|_p \equiv \left(\sum_i |\theta_i|^p\right)^{1/p} \leqslant R \tag{2}$$

for some $0 < p < 2$ and for some $R > 0$. The case $p = 1$ corresponds to the well-known sparseness promotion employed within a Laplacian [21] distribution in Bayesian analysis, or ℓ_1 regularization [7,8] resulting from an associated maximum *a posteriori* analysis [21]. As p gets smaller the signals must be more sparse to satisfy (2) for a given R.

2.2. Random construction of information operator I_n

The signal u may be expressed as a column vector $u = \Psi\theta$, where θ is a column vector composed of coefficients $\{\theta_i\}_{i=1,m}$ and Ψ is an $m \times m$ matrix, the ith column of which is defined by the basis vector ψ_i; the vector u is assumed sparse in the basis Ψ. The CS measurements may be represented by the n-dimensional column vector v, with $v = \Phi\Psi^H u$. The matrix resulting from the product $\Phi\Psi^H$ is responsible for the n projections; Φ is an $n \times m$ matrix, and the CS measurements may now be expressed as $v = \Phi\theta$.

A remarkable result proven by Candès and Tao [19] and Donoho [8] is that if the columns of matrix Φ are generated iid from an underlying distribution (*e.g.* Gaussian or Bernoulli) then the process of measuring v and then recovering u is essentially optimal. Specifically, with "overwhelming probability", when constituting the projection vectors (rows of Φ) in such a random manner, one may recover the underlying signal u with the fewest number of measurements n. This optimality is manifested in the following sense [19]: By using randomly constituted projection vectors, one requires a near-minimal number of measurements n to recover the underlying signal u. The required number of projections is $n \approx N\log(m)$ [8], where recall that N represents the number of significant transform coefficients (if the signal is highly compressible $N \ll m$ and therefore $N\log(m) \ll m$ for large m).

In practice the underlying signal u is recovered as the solution to the convex ℓ_1 regularized inversion

$$\min_g \|\theta(g)\|_{\ell_1} \text{ subject to } \Phi\theta(g) = v = \Phi\theta(u). \tag{3}$$

There have been several algorithms developed to implement this inversion [14,13,9,10,22]. In practice one typically does not know the appropriate N *a priori*, and therefore there may be some uncertainty in selecting n. The inversion algorithm in [13] not only estimates u, but also provides "error bars"; therefore [13] allows one to adaptively determine an appropriate number of CS measurements n, based on a preset error criterion on the recovery of u.

2.3. Orthogonal projections and mutual coherence

While randomly constituted projection vectors may be designed as discussed above, there are other constructions of interest, and of relevance to electromagnetic scattering [23]. For the m-dimensional sparse signal of interest θ Candès and Romberg [20] consider an orthogonal basis B, with $B^H B = mI$, where I is the $m \times m$ identity matrix (Candès and Romberg

[20] chose not to consider a normalized basis for reasons that become apparent below). The basis B may be represented as $B = \Upsilon\Psi$ for orthogonal matrix Υ and with Ψ representing the same sparseness promoting basis as above; an $m \times 1$ complex measurement vector v is constituted as

$$y = B\theta = \Upsilon\Psi\theta = \Upsilon u \tag{4}$$

which is of the same form as for the random projections considered above, but we use the distinct B to underscore that above Φ was constituted via draws from an underlying random variable, while B is the product of two bases (Υ and Ψ); B is also a square $m \times m$ matrix, where Φ is an $n \times m$ matrix, typically with $n \ll m$.

Candès and Romberg [20] have demonstrated that if one *randomly* selects to measure n elements from the vector y, this now constituting the $n \times 1$ compressive sensing measurement v, and n is sufficiently large, with overwhelming probability one may recover the underlying signal u using the same class of inversion algorithms as in (3). A proportionality constant on the required n is

$$\mu(B) = \max_{i,k} |B_{ik}|. \tag{5}$$

As discussed by Candès and Romberg, the form of $\mu(B)$ has important implications for the desired choice of the basis Υ. Specifically, to minimize $\mu(B)$, and hence minimize the number of compressive sensing measurements n, the measurement vectors (rows of Υ) must be "spread out" in the Ψ domain [20]. For this reason $\mu(B)$ is often referred to as the *mutual coherence* and the goal is to design Υ such that $\mu(B)$ is $O(1)$.

3. Exploiting complex target excitations for scattering

The principal application in this paper is a demonstration of how CS may be used to accelerate existing *numerical* electromagnetic scattering codes. To do this, rather than considering plane wave excitation on the target, more-sophisticated incident fields are addressed. Before demonstrating that in Section 5, it is of interest to examine how such excitations may be manifested in *physical* systems, by exploiting multiple scattering in a complex environment. This represents an extension of ideas considered in [23], wherein only radiation (not scattering) was considered. Thus, while the concepts presented here are applied specifically to scattering computations, they may also be exploited when performing physical measurements.

3.1. Excitation fields

We consider two-dimensional scattering to simplifying notation, although the basic construct extends naturally to three-dimensional problems. We desire the signal $u_s(\phi_i, \phi_s, \rho_s, \omega)$, which represents the scattered fields of a target situated in vacuum, with the measurements performed at angular frequency ω, due to a plane wave incident at angle ϕ_i, with the scattered fields observed at angle ϕ_s. The scattered fields are assumed to be observed in the far-zone, at an arbitrary (large) range ρ_s. The compressive sensing analysis seeks to recover $u(\phi_i, \phi_s, \omega)$, which represents the Fourier transform of the currents induced on the target at spectral angle ϕ_s, for incident angle ϕ_i. The desired $u_s(\phi_i, \phi_s, \rho_s, \omega)$ may be recovered from $u(\phi_i, \phi_s, \omega)$ via the free-space Green's function, and in the far-zone

$$u_s(\phi_i, \phi_s, \rho_s, \omega) = \frac{exp(-jk_o\rho_s - j\pi/4)}{4\pi}\sqrt{\frac{2\pi}{k_o\rho_s}}u(\phi_i, \phi_s, \omega). \tag{6}$$

Concerning notation, $u(\phi_i, \phi_s, \omega)$ represents a complex and continuous function of (ϕ_i, ϕ_s, ω); when this function is discretized with respect to (ϕ_i, ϕ_s, ω) the corresponding complex vector is represented as u. Similar notation is employed for the vector of complex CS measurements v. The expression $u(\phi_i, \phi_s, \omega)$ corresponds to the Fourier transform of the currents induced on the target of interest, with ϕ_s representing the spectral angle and ϕ_i the plane wave angle of incidence.

Rather than performing a scattering analysis in vacuum, we assume that the target is surrounded by a complex propagation medium. The objective is to *exploit* the multipath introduced by such an environment to approximate $u(\phi_i, \phi_s, \omega)$ based on a relatively small number of measurements performed in the presence of the heterogeneities, using ideas from compressive sensing.

In the discussion that follows we assume the aforementioned excitation is a line current, for analytical simplicity, but the formulation generalizes to arbitrary two-dimensional sources. In addressing the excitation fields, we consider the source radiating in the presence of the heterogeneous medium, but with the target absent. Specifically, as depicted in Figs. 1 and 2, assume that a contiguous vacuum pocket is surrounded by a heterogeneous propagation environment, and that a line source excitation is positioned at arbitrary point $\boldsymbol{\rho}_e$ outside the vacuum. As a consequence of the complicated propagation environment, the fields within the vacuum arrive at a wide range of angles (typically a continuum of angles). Assuming that the source is operating at frequency ω, let $g(\boldsymbol{\rho}, \boldsymbol{\rho}_e; \omega)$ represent the fields at arbitrary position $\boldsymbol{\rho}$ within the vacuum pocket (the coordinate-system origin is at the center of the vacuum); since the source at $\boldsymbol{\rho}_e$ is a line source, $g(\boldsymbol{\rho}, \boldsymbol{\rho}_e; \omega)$ represents the associated two-dimensional Green's function.

We introduce a window function $w(\boldsymbol{\rho}, \rho_t, \rho_h)$, with $w(|\boldsymbol{\rho}| \leqslant \rho_t, \rho_t, \rho_h) = 1, w(|\boldsymbol{\rho}| \geqslant \rho_h, \rho_t, \rho_h) = 0$, and for $\rho_t \leqslant |\boldsymbol{\rho}| \leqslant \rho_h$ the function $w(\boldsymbol{\rho}, \rho_t, \rho_h)$ tapers to zero in an arbitrary smooth manner (see Fig. 3). The windowed version of the fields within the vacuum are represented as $g_w(\boldsymbol{\rho}, \boldsymbol{\rho}_e; \omega) = g(\boldsymbol{\rho}, \boldsymbol{\rho}_e; \omega)w(\boldsymbol{\rho}, \rho_t, \rho_h)$.

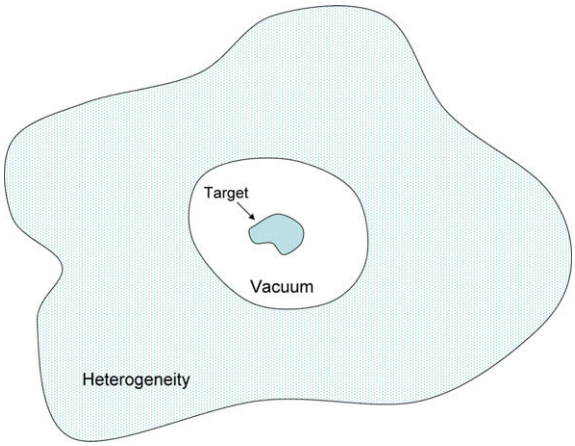

Fig. 1. Schematic of a situated in the presence of a heterogeneous medium. The immediate vicinity of the target is surrounded by vacuum.

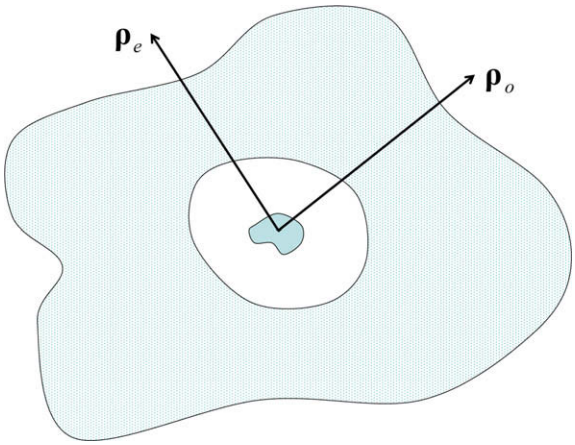

Fig. 2. Location of a line source positioned at $\boldsymbol{\rho}_e$, with the scattered fields observed at $\boldsymbol{\rho}_o$.

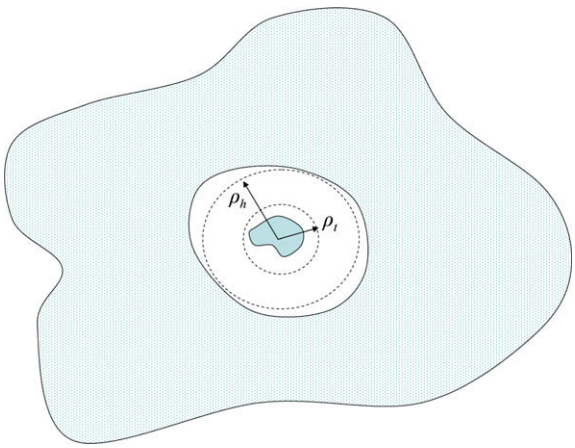

Fig. 3. Depiction of coordinates on window function $w(\boldsymbol{\rho}, \rho_t, \rho_h)$.

The two-dimensional Fourier transform of the windowed fields is defined as

$$\hat{g}_w(\varphi, \boldsymbol{\rho}_e; \omega) = \int_0^{\infty} d\rho \int_0^{2\pi} d\phi \rho g_w(\rho, \phi, \boldsymbol{\rho}_e; \omega) exp[jk_o \rho cos(\phi - \varphi)] \tag{7}$$

with $k_o = \omega/c, c$ is the wave speed in vacuum, φ represents the angle of the spectral component, and the range-angle pair (ρ, ϕ) define the vector $\boldsymbol{\rho}$. Physically, $\hat{g}_w(\varphi, \boldsymbol{\rho}_e; \omega)$ represents the amplitude of a plane wave at frequency $\omega = k_o c$ propagating in the direction φ, due to the source at $\boldsymbol{\rho}_e$, and therefore this is the amplitude of the respective plane wave component associated with the windowed fields $g_w(\boldsymbol{\rho}, \boldsymbol{\rho}_e; \omega)$. The frequency ω and source position $\boldsymbol{\rho}_e$ are assumed fixed, and therefore $\hat{g}_w(\varphi, \boldsymbol{\rho}_e; \omega)$ is a function of the spectral angle (plane wave propagation direction) φ.

Note that for a fixed source, through exploitation of the complex propagation medium, one may effectively constitute excitation plane waves propagating at a continuum of angles in the region within which the target will reside; by contrast, in the absence of the heterogeneity a single propagation direction will dominate, for a fixed source location (assuming the source is distant from the origin).

The windowed source currents may be recovered via an inverse Fourier transform

$$g_w(\boldsymbol{\rho}, \boldsymbol{\rho}_e; \omega) = \frac{k_o}{4\pi^2} \int_0^{2\pi} d\varphi \hat{g}_w(\varphi, \boldsymbol{\rho}_e; \omega) exp[-jk_o \rho cos(\phi - \varphi)] \tag{8}$$

assuming that there are no evanescent fields in $g_w(\boldsymbol{\rho}, \boldsymbol{\rho}_e; \omega)$ and hence that $\hat{g}_w(\varphi, \boldsymbol{\rho}_e; \omega)$ exists in the spectral domain on a circle of radius k_o. The expression in (8) underscores that the spectral form of the source excitation $\hat{g}_w(\varphi, \boldsymbol{\rho}_e; \omega)$ is only a function of the angle φ. Thus motivated, it will prove convenient in Section 3.4 to constitute a discretized form of $\hat{g}_w(\varphi, \boldsymbol{\rho}_e; \omega)$, discretized with respect to the angle $\varphi \in [0, 2\pi]$. Specifically, let ξ_{ρ_e} represent an $\sqrt{m}$ dimensional *complex* column vector, corresponding to $\hat{g}_w(\varphi, \boldsymbol{\rho}_e; \omega)$ uniformly sampled at $\sqrt{m}$ angular points φ. The vector ξ_{ρ_e} represents the weights of plane waves incident upon the target due to a source at $\boldsymbol{\rho}_e$, at an $\sqrt{m}$-dimensional set of discrete plane wave propagation directions (angles). Recall that it is assumed that $\sqrt{m}$ is an integer.

3.2. Radiation from induced source

Fields incident upon a scatterer induce currents on the target surface (and/or within the target), and the scattered fields are radiated by this source, with radiation taking place in the presence of the background medium. Therefore, to consider the scattering problem, we first address radiation from a general source, radiating from within the vacuum pocket in Fig. 1 (the target will reside within this region). Specifically, assume that $i(\boldsymbol{\rho}', \omega)$ represents a source at frequency ω, residing within the pocket vacuum region, and therefore $i(|\boldsymbol{\rho}'| \geqslant \rho_t, \omega) = 0$. Let $g(\boldsymbol{\rho}_o, \boldsymbol{\rho}'; \omega)$ represent the Green's function for a line source located at $\boldsymbol{\rho}'$, for $|\boldsymbol{\rho}'| \leqslant \rho_t$, and the associated fields are observed at any point $\boldsymbol{\rho}_o$. The fields at $\boldsymbol{\rho}_o$ due to the source $i(\boldsymbol{\rho}', \omega)$, radiating in the presence of the heterogeneities, may therefore be expressed as

$$f(\boldsymbol{\rho}_o, \omega) = \int d\boldsymbol{\rho}'^2 i(\boldsymbol{\rho}', \omega) g(\boldsymbol{\rho}_o, \boldsymbol{\rho}'; \omega). \tag{9}$$

Because of the finite support of the current, we recall the window function $w(\boldsymbol{\rho}, \rho_t, \rho_h)$ introduced above, and window the Green's function as $g_w(\boldsymbol{\rho}_o, \boldsymbol{\rho}'; \omega) = g(\boldsymbol{\rho}_o, \boldsymbol{\rho}'; \omega) w(\boldsymbol{\rho}', \rho_t, \rho_h)$. Using Parseval's theorem, (9) may be expressed as

$$f(\boldsymbol{\rho}_o, \omega) = \frac{k_o}{4\pi^2} \int_0^{2\pi} d\varphi \hat{i}(\varphi, \omega) \hat{g}_w(\boldsymbol{\rho}_o, \varphi + \pi; \omega), \tag{10}$$

where $\hat{i}(\varphi, \omega)$ and $\hat{g}_w(\boldsymbol{\rho}_o, \varphi; \omega)$ are spectral forms of the source current and windowed Green's function, respectively, defined similarly to (7), and in (10) it is assumed that the evanescent components of the spectral currents do not contribute to the fields observed at position $\boldsymbol{\rho}_o$.

3.3. Scattering from target embedded in heterogeneity

Let $u(\phi_i, \varphi, \omega)$ represent the two-dimensional Fourier transform of the current induced on the target at spectral angle φ, due to a *unit-amplitude* plane wave incident *in vacuum* at angle ϕ_i and frequency ω. If we ignore multiple interactions between the target and the background heterogeneities in Fig. 1 (this is termed the Born approximation [24], and it is often appropriate for heterogeneities sufficiently distant from the target), then the Fourier transform of the induced currents on the target, due to the excitation $g_w(\boldsymbol{\rho}, \boldsymbol{\rho}_e; \omega)$ discussed in Section 3.1, may be expressed as

$$\hat{i}(\varphi, \omega) \approx \int_0^{2\pi} d\phi_i u(\phi_i, \varphi, \omega) \hat{g}_w(\phi_i, \boldsymbol{\rho}_e; \omega), \tag{11}$$

where we recall that $\hat{g}_w(\phi_i, \boldsymbol{\rho}_e; \omega)$ represents the amplitude of plane wave component propagating at angle ϕ_i within the overall excitation field $g_w(\boldsymbol{\rho}, \boldsymbol{\rho}_e; \omega)$. In the subsequent analysis we assume the approximation in (11) to be accurate (thereby assuming that the Born approximation is accurate), with this issue revisited in Section 3.6.

Let the $\sqrt{m} \times \sqrt{m}$ matrix U represent a sampled version of $u(\phi_i, \phi_s, \omega)$, with the columns representing $\sqrt{m}$ samples with respect to $\phi_i \in [0, 2\pi]$, and the rows representing $\sqrt{m}$ samples with respect to $\phi_s \in [0, 2\pi]$ (when "unwrapped" U represents the vector u). From (11) a discretized form of the induced current (at $\sqrt{m}$ discrete $\varphi = \phi_s$) may be expressed as

$$\hat{i} \approx \Delta_{\phi_i} \xi_{\rho_e}^T U, \tag{12}$$

where now $\hat{i}$ is in the form of an $\sqrt{m}$-dimensional complex row vector, and Δ_{ϕ_i} represents the sample rate of the angle $\phi_i \in [0, 2\pi]$. Eq. (12) represents the induced target current in the spectral domain as a weighted sum of spectral currents, with the weighting (complex vector) ξ_{ρ_e} defined by the amplitude of $\sqrt{m}$ plane waves propagating at discrete angles $\phi_i \in [0, 2\pi]$.

Using (10), the fields scattered from the target situated within the presence of the heterogeneity, as observed at $\boldsymbol{\rho}_o$, is given approximately as

$$v(\boldsymbol{\rho}_o, \boldsymbol{\rho}_e, \omega) \approx \frac{k_o \Delta_{\phi_i} \Delta_{\phi_s}}{4\pi^2} \xi_{\rho_e}^T U \zeta_{\rho_o}, \tag{13}$$

where ζ_{ρ_o} represents ξ_{ρ_o} with a shift of the angle φ by π, commensurate with (10); $v(\boldsymbol{\rho}_o, \boldsymbol{\rho}_e, \omega)$ is a complex number corresponding to a measurement for a source at $\boldsymbol{\rho}_e$ and observer at $\boldsymbol{\rho}_o$. A total of n such measurements (for n combinations of the pair $(\boldsymbol{\rho}_e, \boldsymbol{\rho}_o)$) yields an n-dimensional *complex* CS vector v. The approximation in (13) is manifested by discretization with the angles ϕ_i and ϕ_s, and it is exact in the limit $\Delta_{\phi_i} \to 0$ and $\Delta_{\phi_s} \to 0$.

3.4. Compressive sensing perspective

The matrix U defines the induced target spectral current $u(\phi_i, \phi_s)$ at $\sqrt{m} \times \sqrt{m}$ discrete sets of angles (ϕ_i, ϕ_s), and rather than viewing it as a matrix, it may be "unwrapped" to constitute an m-dimensional column vector u. Further, the linear relationship between the (single) compressive measurement $v(\boldsymbol{\rho}_o, \boldsymbol{\rho}_e, \omega)$ and u, as defined by (13), may be expressed in terms of the $m \times 1$ dimensional vector σ_{ρ_o, ρ_e}, and therefore

$$v_{\rho_o, \rho_e} = \sigma_{\rho_o, \rho_e}^T u \tag{14}$$

with v_{ρ_o, ρ_e} corresponding to the complex measured data.

Assume n such compressive sensing measurements are performed, at n different pairs of source-observation positions $(\boldsymbol{\rho}_o, \boldsymbol{\rho}_e)$, then the compressive sensing measurements at frequency ω may be expressed as

$$v = \Sigma u. \tag{15}$$

All discussions above have assumed operation at a single frequency ω. The discussion may be extended to multiple frequencies. Because of the assumed linear scattering, the different frequencies may be characterized independently, and therefore the matrix Σ generalizes to a larger matrix; this matrix is block diagonal with each block corresponding to a particular frequency and of the form discussed above. In this context, we may similarly generalize the single frequency vectors v and u by concatenating such vectors associated with different frequencies.

The function $u(\phi_i, \phi_s, \omega)$ is generally a smooth function of variables (ϕ_i, ϕ_s, ω), which implies that a discrete cosine transform (DCT) or wavelet (or other appropriate orthonormal) transform of the discretized $u(\phi_i, \phi_s, \omega)$ should be sparse, implying that the associated transform coefficients should have a large fraction of negligibly small coefficients.

Letting θ represent the vector of m transform coefficients, and letting Ψ represent the $m \times m$ basis in which u is sparse, then $u = \Psi\theta$ and

$$v = \Sigma\Psi\theta = \Phi\theta. \tag{16}$$

3.5. Properties of the matrix Φ and choice of Ψ

We now carefully examine the properties of the rows of Σ in (16), these constituting the projection vectors manifested by the two-way Green's function projections. The projection associated with source point $\boldsymbol{\rho}_e$ and observation point $\boldsymbol{\rho}_o$ may be represented via (13) as

$$v(\boldsymbol{\rho}_o, \boldsymbol{\rho}_e) \approx \frac{k_o \Delta^2}{4\pi^2} \sum_{i=1}^{\sqrt{m}} \sum_{k=1}^{\sqrt{m}} u[(i\Delta - \phi_{ic}), (k\Delta - \phi_{sc})] \hat{g}(\boldsymbol{\rho}_o, (\pi + i\Delta - \phi_{ic})) \hat{g}(\boldsymbol{\rho}_e, (k\Delta - \phi_{sc})), \tag{17}$$

where we assume that the sample rate in ϕ_i and ϕ_s is the same and set at Δ, and explicit dependence on ω has been removed to simplify notation; ϕ_{ic} and ϕ_{sc} represent centering offsets (constants) to align the angle-dependent function in discretized form. Therefore, in the limit $\Delta \to 0$ the inner product between two different rows of Σ may be expressed as

$$\langle \sigma_{\rho_{o1}, \rho_{e1}}, \sigma_{\rho_{o2}, \rho_{e2}} \rangle \propto \int_0^{2\pi} d\phi_i \hat{g}_w(\phi_i, \boldsymbol{\rho}_{e1}) \hat{g}_w^*(\phi_i, \boldsymbol{\rho}_{e2}) \int_0^{2\pi} d\phi_s \hat{g}_w(\phi_s, \boldsymbol{\rho}_{o1}) \hat{g}_w^*(\phi_s, \boldsymbol{\rho}_{o2}). \tag{18}$$

The expressions $\int_0^{2\pi} d\phi_i \hat{g}_w(\phi_i, \boldsymbol{\rho}_{e1}) \hat{g}_w^*(\phi_i, \boldsymbol{\rho}_{e2})$ and $\int_0^{2\pi} d\phi_s \hat{g}_w(\phi_s, \boldsymbol{\rho}_{o1}) \hat{g}_w^*(\phi_s, \boldsymbol{\rho}_{o2})$ correspond to time-reversal operators [25]. Specifically, the former corresponds to a line source excitation at $\boldsymbol{\rho}_{e2}$ radiating in the presence of the medium; the fields inside the vacuum pocket (see Fig. 3) are then complex conjugated (time-reversed, in the time domain) and then radiated into the medium, with observation at the point $\boldsymbol{\rho}_{e1}$. A similar phenomenon is associated with the other term in (18). To satisfy the requirement that the rows of Σ be orthogonal, we should place the transmitted-receiver pairs $(\boldsymbol{\rho}_e, \boldsymbol{\rho}_o)$ such that when the sensor positions are changed (each pair corresponding to one row in Σ), then the integrals in (18) should be relatively small (relative to when (18) represents co-located sensors). The more complicated the propagation medium, the more tightly can be the inter-sensor spacing, while still satisfying the required near-orthogonality properties of the rows of Σ.

The above discussion demonstrates that if the sensors are situated properly, the required orthogonality (or near-orthogonality) properties of the CS projections is realized (recall Section 2.3). Further, if the sensor positions are selected randomly (within the constraint that they satisfy near-orthogonality), the matrix Σ satisfies the desired properties (orthogonal rows) for construction of a CS matrix Φ. The second issue concerns the mutual coherence (see (5)) between Σ and the basis Ψ in which u is sparse (or near-sparse) – this will dictate the number of different sensor positions that must be considered to constitute v.

It is desirable to choose Ψ such that any row in Σ is "spread out" in the orthonormal space defined by Ψ [20], thereby minimizing the mutual coherence between Σ and Ψ. On the other hand, the Ψ must be selected such that u is highly compressible in this basis, such that S is as small as possible, since the number of required projections is also proportional to S. In most wave propagation problems the Green's functions in (18) tend to be spread out in a DCT basis, and therefore the DCT is a good choice for Ψ with the goal of minimizing the mutual coherence. Moreover, we have found that scattering from most targets yields an angle-dependent signal u that is highly compressible in a DCT basis. Therefore, in the examples presented below we typically let Ψ correspond to the DCT basis.

3.6. Revisiting approximations

In Section 3.1 we commenced by stating the goal of recovering $u_s(\phi_i, \phi_s, \rho_s, \omega)$ for a large range of $(\phi_i, \phi_s, \rho_s, \omega)$, where $u_s(\phi_i, \phi_s, \rho_s, \omega)$ represents the complex scattered field of a target situated in vacuum, as viewed in the far-zone at (ϕ_s, ρ_s), due to plane wave excitation at angle ϕ_i and frequency ω. The compressive sensing analysis above sought to recover $u(\phi_i, \phi_s, \omega)$, which represents the Fourier transform of the associated induced currents, at spectral angle ϕ_s. The desire for $u_s(\phi_i, \phi_s, \rho_s, \omega)$ motivated assuming the Born approximation in (11). However, if the Born approximation is not valid, this does not undermine the overarching compressive sensing analysis. It simply implies that the associated scattered fields also include effects of the induced current introduced by interaction with the heterogeneous background. Hence, rather than recovering the induced current of the target due to scattering within a vacuum, the effects of the heterogeneity are also included (although, as indicated, these are often weak).

4. Accelerating existing scattering analysis tools

The discussion in the previous section demonstrated that near-orthogonal projection measurements of the type required for CS may be manifested by exploiting multiple scattering in complex environments. While this may be of practical importance for inferring a target signature u based on scattering measurements, the significant complication is that one needs to accurately know the projection matrix Φ, which implies knowing the media Green's function. Ideas along these lines were considered in [23], although there radiation problems were considered, rather than scattering. As demonstrated below, when interested in *computational* electromagnetic scattering, one may explicitly design the matrix Φ, and therefore CS inversion for the multi-static scattered fields is readily possible. As demonstrated below, this has the potential to significantly accelerate multi-static scattering calculations.

4.1. Setup of CS scattering computations

Most linear scattering analyses result in a matrix equation of the form [15]

$$Zi = e, \tag{19}$$

where i represents a column vector of basis function coefficients to be solved for, and the column vector e represents the known source, or excitation. If the analysis involves N_b basis function coefficients, then i and e are complex vectors of dimension N_b, and Z is an $N_b \times N_b$ complex matrix. When the dimensions of the target become large with respect to excitation wavelength (most such analyses are performed one frequency or wavelength at a time), then the number of basis functions N_b may become quite large. Therefore, the order N_b^2 computational cost associated with filling Z, and the cost of performing the matrix inversion for i, become prohibitive. Once i is computed for a particular excitation e, the scattered fields observed at different angles with respect to the target may be computed efficiently [15]. Therefore, the principal computational bottleneck is manifested in forming and solving (19) for a particular angle of incidence. This computational challenge has motivated development of techniques that allow (19) to be solved more efficiently than a naive direct solution, with the fast-multipole method [17,16,18] constituting an important example. These latter techniques require $O(N_b log N_b)$ computational cost to solve for i, and $O(N_b)$ computational cost to solve for the associated scattered fields after i is obtained. Even with these fast techniques, forming and solving (19) for the unknown i becomes computationally prohibitive as the size of the target increases relative to wavelength, *i.e.* with increasing N_b.

The analysis in (19) may be viewed as a *computational* sensing experiment: given the excitation e, the goal is to perform a computational "experiment" to estimate i, and from i the scattered field. Hence, the same ideas from compressive *sensing*, which have typically been applied to physical experiments, may also be applied to computational experiments. One may therefore ask the following question: Is it possible to employ CS to reduce the number of times we must solve (19), and, based upon this reduced set of calculations, can the full multi-static scattering profile be recovered? In this context the

"sensing" part of CS corresponds to executing a numerical computation, and the objective is to employ CS to reduce the number of required computations.

To perform numerical scattering computations in a CS mode, one may perform relatively simple modifications to existing numerical models that constitute and solve matrices of the form $Zi = e$. Specifically, rather than assuming plane wave excitation, the excitation e in (19) is composed of a linear combination of plane waves, with the weights on this superposition (here) drawn iid from a Gaussian random variable, with zero mean and unit variance; based upon the CS theory summarized in Section 2, one may also consider alternative random variables. In the computations presented in Section 5, the plane wave incidence (excitation) angle θ_e is sampled uniformly 128 times over $0^\circ \leqslant \theta_e \leqslant 180^\circ$, and each of the 128 plane waves is weighted by a unique draw from the aforementioned random variable, and then all plane waves are superposed to constitute *one* excitation e; importantly, using an e so constituted requires no more cost to solve (19) than if e corresponds to a plane wave. Once i is computed for a given e, the scattered fields are also computed in a CS mode, corresponding to a weighted sum of the scattered fields at different angles. In Section 5, 128 uniformly spaced scattering angles θ_s are considered over the range $0^\circ \leqslant \theta_s \leqslant 180^\circ$, with the weights again iid draws from the same random variable. Within the computational electromagnetic scattering engine, this weighted sum of fields from 128 scattering angles are computed at once, with no more computational cost than observing the scattered fields at a single scattering angle θ_s. This process yields a single CS measurement (a single component of v). Let N_e represent the number of different randomly constituted excitations v considered (defined by different random variable draws), and *for each* we consider N_s random projections as a function of scattering angle, for a total of $N_e \times N_s$ CS computations. Since, as discussed above, the solution in (19) for i is the computational bottleneck (at best $O(N_b log N_b)$), the CS computations will be performed with the goal of minimizing N_e, recognizing that there is negligible additional cost associated with increasing N_s (recall that after i is computed, the scattered fields are computed with $O(N_b)$ complexity).

4.2. Inversion for desired multi-static scattered fields

As a consequence of the aforementioned CS-based scattering computations, we constitute an n-dimensional complex vector v (where here $n = N_e \times N_s$, using notation from above). Our goal is to infer from v the scattered fields as a function of discrete plane wave excitation angles and discrete observation angles, with the associated matrix of scattered fields represented as u. For the n-dimensional vector v, and the m elements in the matrix u, we desire an algorithm $A_n : \mathbf{C}^n \rightarrow \mathbf{C}^m$, as discussed in Section 2.

Let u be the desired multi-static scattering matrix at a given frequency, where one dimension represents the plane wave excitation angle and the other dimension represents the scattering angle; there are assumed $\sqrt{m}$ angles in each of these dimensions, where $\sqrt{m}$ is assumed to be an integer. Let the set of column vectors ψ_k for $k = 1, \ldots, \sqrt{m}$ represent an orthonormal basis in a vector space of dimension $\sqrt{m}$, and therefore we may represent the matrix u as

$$u = \sum_{j=1}^{\sqrt{m}} \sum_{k=1}^{\sqrt{m}} \psi_j \psi_k^T \theta_{j,k}. \tag{20}$$

where $\theta_{j,k}$ represents the complex (scalar) weight on the two-dimensional orthonormal basis $\psi_j \psi_k^T$. Our goal is to infer $\theta_{j,k}$ from the compressive computations v, under the assumption that the m weights $\theta_{j,k}$ are sparse (most $\theta_{j,k}$ may be set to zero, with negligible impact on the reconstruction of u). Note that each $\psi_j \psi_k^T$ corresponds to one (of m) column in the matrix Ψ discussed in Section 2.

We further let $\eta_{e,l}$ represent a vector of dimension $\sqrt{m}$, corresponding to the lth set of randomly constituted weights on the $\sqrt{m}$ plane wave excitation angles; the vector $\eta_{s,k}$ is similarly defined for the lth set of randomly constituted weights on the $\sqrt{m}$ scattering angles. The lth compressive computation (lth component of v) may be expressed as

$$v(l) = \eta_{e,l}^T u \eta_{s,l} = \sum_{j=1}^{\sqrt{m}} \sum_{k=1}^{\sqrt{m}} \eta_{e,l}^T \psi_j \psi_k^T \eta_{s,l} \theta_{j,k}. \tag{21}$$

Therefore, the complex vector of n such compressive computations may be expressed as

$$v = \Phi \theta, \tag{22}$$

where θ is an m-dimensional vector composed of the components $\{\theta_{j,k}\}$, for $j = 1, \ldots, \sqrt{m}$ and $k = 1, \ldots, \sqrt{m}$, and the lth row of Φ is defined by the components $\{\eta_{e,l}^T \psi_j \psi_k^T \eta_{s,l}\}$, again for $j = 1, \ldots, \sqrt{m}$ and $k = 1, \ldots, \sqrt{m}$. Note that in many cases the components $\{\eta_{e,l}^T \psi_j \psi_k^T \eta_{s,l}\}$ may be computed very efficiently. For example, if ψ_k for $k = 1, \ldots, \sqrt{m}$ corresponds to a DCT or wavelet basis, then the components $\{\eta_{e,l}^T \psi_j \psi_k^T \eta_{s,l}\}$ may be computed efficiently using a fast Fourier or wavelet transform, respectively, of the randomly constituted matrix $\eta_{e,l} \eta_{s,l}^T$.

The vector θ is of dimension m, and we assume n CS computations, with $n \ll m$. Therefore, the matrix Φ is of dimension $n \times m$, and $v = \Phi \theta$ is an under-determined matrix equation. As indicated in Section 2, the algorithm $A_n : \mathbf{C}^n \rightarrow \mathbf{C}^m$ addresses this problem by imposing the constraint that the signal of interest u is compressible in the basis $\{\psi_j \psi_k^T\}$ for $j = 1, \ldots, \sqrt{m}$ and $k = 1, \ldots, \sqrt{m}$ (the vector θ is sparse). There have been many different algorithms developed to perform this regularized inversion [9–11,7,12,13,**?**], and here we employ [13].

4.3. Exploitation of reciprocity

As discussed above, u is an $\sqrt{m} \times \sqrt{m}$ complex matrix, where the (i,j) component $u(i,j)$ represents the far-zone scattered field at angle j due to plane wave incidence at angle i. Due to reciprocity, we have $u(i,j) = u(j,i)$. In the compressive sensing inversion discussed above we exploit the fact that u is compressible in an appropriate basis. We would like to also exploit the fact that u has the aforementioned symmetry property. For arbitrary projections of the type discussed above, the kth CS-type electromagnetic computation may be expressed in the form

$$v(k) = \sum_{i=1}^{\sqrt{m}} \sum_{j=1}^{\sqrt{m}} a_k(i,j) u(i,j), \tag{23}$$

where $a_k(i,j)$ represents the cumulative amplitude weighting $u(i,j)$ for projection k. As a consequence of reciprocity, we may also express (23) as

$$v(k) = \sum_{i=1}^{\sqrt{m}} \sum_{j=1}^{\sqrt{m}} \hat{a}_k(i,j) u(i,j), \tag{24}$$

where $\hat{a}_k(i,j) = a_k(i,j) + \Delta(i,j)$ and $\hat{a}_k(j,i) = a_k(j,i) - \Delta(i,j)$, for arbitrary $\Delta(i,j)$. Therefore, we may perform n CS-based electromagnetic computations $\{v(k)\}_{k=1,n}$, with associated projection weights $a(i,j)$ as in (23), and for arbitrary $\Delta(i,j)$ these same computations may be used to represent an additional n computations of the form (24). The fact that both (23) and (24) are solved simultaneously implicitly imposes the known reciprocity associated with u. In all results presented below, this concept is employed, and the $\Delta(i,j)$ are generated as i.i.d. draws from the normal distribution $\mathcal{N}(0,1)$. Therefore, when discussing n computations below for a given analysis, a total of $2n$ effective computations were employed when performing inversion.

5. Example results

To demonstrate the concepts elucidated above we consider the numerical analysis of electromagnetic scattering from the target in Fig. 4. Scattering from this target is analyzed using the multi-level fast-multipole method (MLFMM) technique discussed in [18]. To simplify the analysis, the calculations were performed at a fixed azimuthal angle $\phi_i = \phi_s = 0^\circ$, and the incidence and scattering angles were varied from $0^\circ \leqslant \theta_e \leqslant 180^\circ$ and $0^\circ \leqslant \theta_s \leqslant 180^\circ$. The MLFMM code was run with plane wave incidence to sample θ_e 128 times, and the far-zone scattered fields were computed at 128 angles θ_s; these scattered fields provide a reference solution for the CS-based computations. The real and imaginary parts of the normalized scattered fields are depicted in Fig. 6, where the fields are normalized with respect to $exp(-jk_o r)/r$, where r is the range from the target center to the (distant) receiver.

As a brief aside, we provide justification now for choosing the DCT as the basis Ψ in the CS analysis presented here. In Fig. 5, we compare the sparseness with which the data in Fig. 4 are rendered for different Ψ. In Fig. 5 are shown the ordered amplitudes when Ψ corresponds to a discrete Fourier transform, a Harr wavelet [1], and a DCT. For the scattering data considered, the DCT provides the sparsest representation, and therefore this has been selected for all CS results presented here. However, as discussed in the Conclusions, further research is of interest concerning the selection of Ψ for scattering computations and measurements.

In Figs. 7 and 8 are shown, respectively, the CS-reconstructed real and imaginary parts of the scattered fields, for which one may compare to the reference solution in Fig. 6. In these computations the number of randomly constituted excitations was fixed at $N_e = 16$, and for each excitation the number of different random projections of the scattered fields was $N_s = 16, N_s = 32$ and $N_s = 64$. The number of complex basis function coefficients was $N_b = 20016$ (this is a relatively small number of unknowns, selected for efficient computation of the reference solution in Fig. 6). While the results for $N_s = 8$ (not shown) are reasonably good, they are substantially worse than those in Figs. 7 and 8. We observe from Figs. 7 and 8 that the CS-based MLFMM computations and associated CS reconstructions are in good agreement with the "truth" in Fig. 6 (a quantitative comparison is provided below).

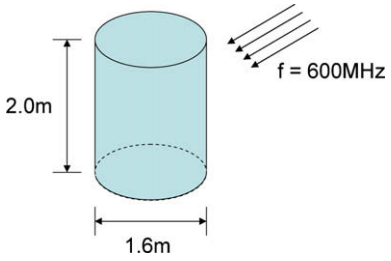

Fig. 4. Finite dielectric cylindrical target considered in three-dimensional fast-multipole electromagnetic scattering calculation. The target is a lossless dielectric with dielectric constant $\epsilon_r = 2$.

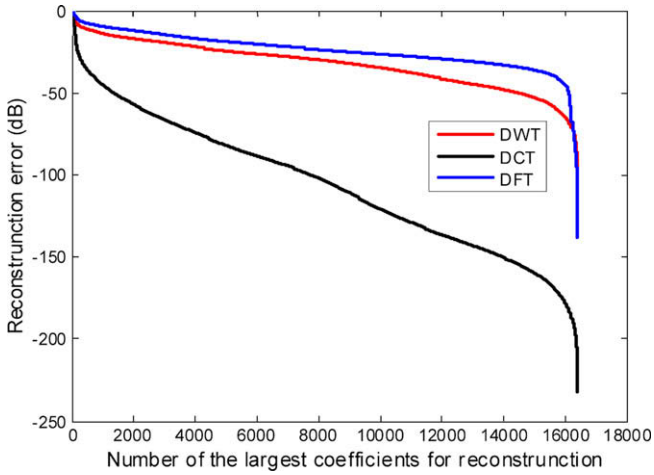

Fig. 5. Comparison of the ordered basis function weights (magnitude) for the scattering data considered in Fig. 6, for Ψ defined by a discrete Fourier, discrete cosine and Harr wavelet basis.

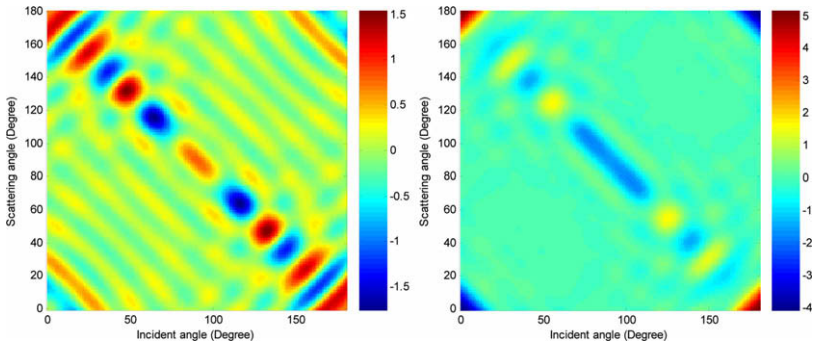

Fig. 6. Real (left) and imaginary (right) parts of the normalized scattered fields, as computed via a reference MLFMM [18] computation, with plane wave excitation and the scattered fields observed in the far-zone, as a function of scattering angle θ_s. The scattered fields are normalized with respect to $exp(-jk_o r)/r$.

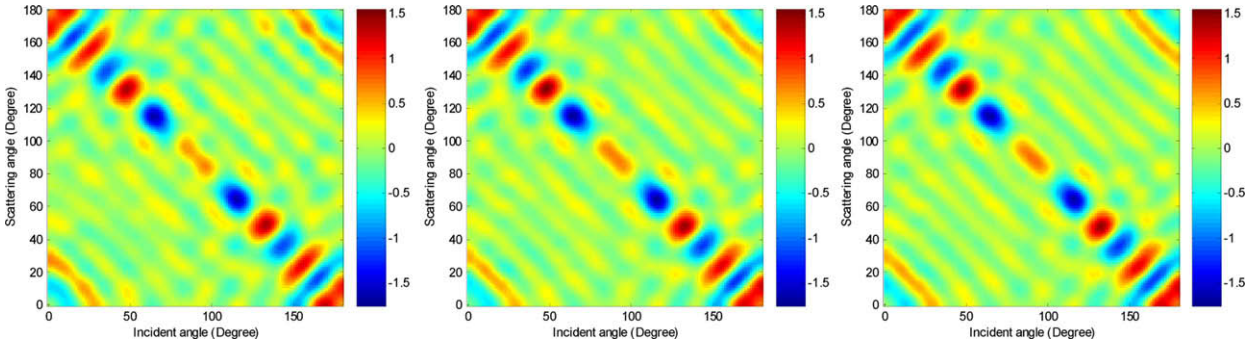

Fig. 7. Real part of the normalized scattered fields, as estimated by compressive sensing. The CS calculations were performed with $N_e = 16$ random excitations, and the number of random CS scattering computations considered is $N_s = 16$ (left), $N_s = 32$ (center) and $N_s = 64$ (right). The scattered fields are normalized with respect to $exp(-jk_o r)/r$.

To provide a comparison of the accuracy of the CS reconstructions, in Fig. 9 is shown the real part of the normalized scattered field, for plane wave excitation at $N_e = 16$ angles over $0^\circ \leqslant \theta_e \leqslant 180^\circ$, and with the scattered field observed at N_s different discrete angles (as in conventional scattering computations) over $0^\circ \leqslant \theta_s \leqslant 180^\circ$; as in the CS computations, we consider $N_s = 16$, $N_s = 32$ and $N_s = 64$. The computational cost for this analysis is the same as that associated with the CS-based analysis in Fig. 7. Although not shown here, for brevity, the imaginary component of these scattered fields, based on linear interpolation of the uniformly sampled results in θ_e and θ_s, have a similar level of accuracy when compared to the

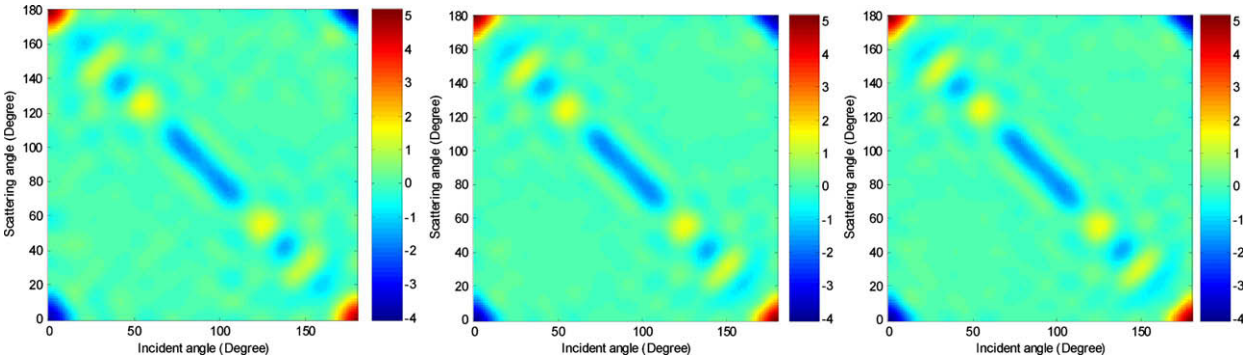

Fig. 8. Imaginary part of the normalized scattered fields, as estimated by compressive sensing. The CS calculations were performed with $N_e = 16$ random excitations, and the number of random CS scattering computations considered is $N_s = 16$ (left), $N_s = 32$ (center) and $N_s = 64$ (right). The scattered fields are normalized with respect to $exp(-jk_o r)/r$.

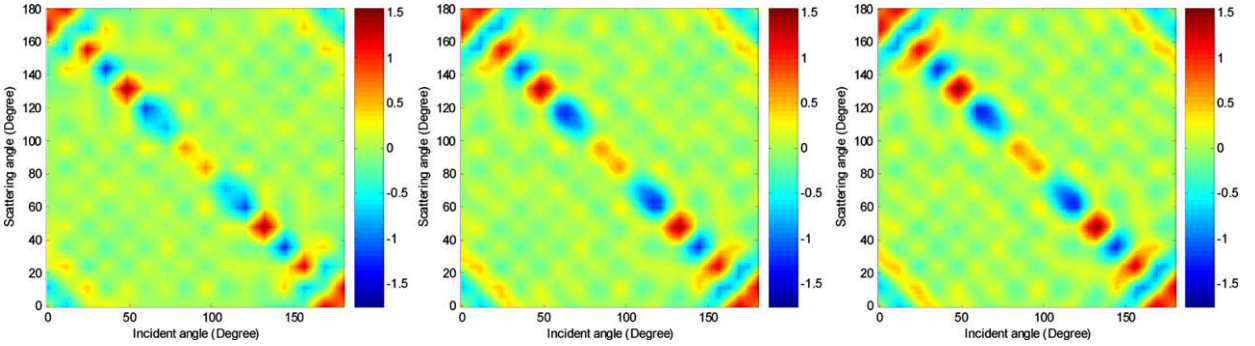

Fig. 9. Normalized scattered fields (real part) computed using random $N_e = 16$ plane wave incident angles uniformly sampled over the range $0^\circ \leqslant \theta_e \leqslant 180^\circ$, and the scattered fields are uniformly sampled at $N_s = 16$ (left), $N_s = 32$ (center) and $N_s = 64$ (right) scattering angles, over $0^\circ \leqslant \theta_e \leqslant 180^\circ$. Linear interpolation is used to estimate the scattered fields at angles θ_e and θ_s for which the numerical scattered fields were not explicitly analyzed.

Table 1
The error $\|I_{est} - I_{ref}\|_2/\|I_{ref}\|_2$, where I_{est} is the estimated (θ_e, θ_s)-dependent scattered field and I_{ref} is the associated reference solution. The results for the error on the real and imaginary part of the scattered fields are denoted "real, imaginary".

	$N_s = 16$	$N_s = 32$	$N_s = 64$
Uniform sampling	0.51, 0.35	0.35, 0.23	0.31, 0.20
Gaussian CS	0.24, 0.21	0.16, 0.11	0.12, 0.10
Bernoulli CS	0.41, 0.28	0.26, 0.19	0.17, 0.13

CS-based results in Fig. 8. The computation of each CS analysis, for a given random projection on excitation and on receive, is exactly of the same complexity as when plane wave excitation is considered, and the scattered fields are observed at a single angle of observation (the CS inversion is performed in seconds in Matlab, and therefore this part of the analysis is a tiny fraction of the time required for the MLFMM scattering analysis).

To provide a quantitative measure of the difference between the CS-computed and traditionally computed (plane wave excitation, and observation at discrete scattering angles), we consider the error $\|I_{est} - I_{ref}\|_2/\|I_{ref}\|_2$, where I_{est} is the estimated (θ_e, θ_s) dependent scattered field (complex) and I_{ref} is the associated reference solution depicted in Fig. 6. The I_{est} is estimated in two different ways, each requiring the same computational cost: (i) the CS-based approach with results reflected in Figs. 7 and 8, and (ii) the "traditional" approach with uniform sampling in (θ_e, θ_s) with results depicted (real part) in Fig. 9. In Table 1 these errors are shown, for $N_e = 16$ source excitations, and for $N_s = 16, N_s = 32$ and $N_s = 64$. It is observed that the CS-based results are significantly more accurate than the corresponding uniform-sampled results. To realize accuracy commensurate with the CS solution, the uniformly sampled results require one to consider $N_e = 32$ excitations, which more than doubles the computational cost.

In Table 1, we present two sets of CS results. The Gaussian CS results employ projection vectors defined by draws from a Gaussian distribution, as utilized in all other examples considered above. As a comparison, we also consider projection vectors that have amplitudes ± 1, where both values are drawn with probability 0.5 (Bernoulli). The latter projections yield CS

results that are generally worse than the Gaussian-defined projections, particularly for a relatively small number of computations. This is attributed to the fact that the ± 1 alphabet is clearly more restrictive relative to draws from a Gaussian distribution. Since there is no computational difference in employing Gaussian or Bernoulli-defined projections, the former is preferred (based on all examples we have considered thus far).

In the traditional uniform-sampled results, linear interpolation was used to extrapolate to angles θ_e and θ_s not explicitly considered via the MLFMM analysis. Therefore, it is possible that the results of the uniform-sampled analysis may be improved by considering a more-sophisticated regression model (*e.g.* splines or a polynomial model). Therefore, the CS results considered here may be viewed from two perspectives: (i) as compared to simple linear interpolation on a uniformly sampled lattice in θ_e and θ_s, the CS results yield improved accuracy with the same computational cost and (ii) the CS analysis may be viewed as integrating the scattering computations with the regression, with the CS inversion providing a smooth and accurate representation of the scattered fields for a finely sampled lattice in θ_e and θ_s.

6. Conclusions

Compressive sensing has been examined as a framework for efficiently performing scattering computations. In the context of a numerical scattering analysis, one typically considers plane wave excitation, with the scattered fields computed in the far field, one angle at a time. From the perspective of CS, the computations are performed using an excitation that is a random combination of plane waves, and the scattered fields are viewed simultaneously at all angles, with the angle-dependent scattered fields projected onto a random vector. The computational cost of a CS analysis is exactly the same as that of a traditional analysis, for which fixed angles of incidence and scattering are considered. The results presented demonstrated that at minimum the CS computations may be viewed as combining the scattering analysis with a regression model, to yield a smooth and highly accurate representation of the scattered fields as a function of angle, with a resolution far superior than that associated with uniform sampling at the same computational cost. The results also demonstrated that the CS-based results are more accurate than those using uniform sampling and simple linear interpolation. We also demonstrated that *physical* CS measurements of this type may be performed by exploiting complex propagation in a complex media. However, in this setting one requires the media Green's function to perform CS inversion.

The work presented here constitutes an introduction of CS to the problem of performing a scattering analysis, and therefore there are more open questions for future research than there are problems solved here. As a sample of open research issues, we discuss the following:

In the context of the MLFMM scattering computations, the CS matrix Φ was constituted by drawing samples from an underlying random variable. While this framework has been demonstrated to give good results, and is blessed with good theoretical properties [8], it has recently been demonstrated that if the underlying signal u is structured, improved performance may be achieved if the Φ matrix is constituted adaptively, sequentially [13]. Noting the relatively highly structured form of angle-dependent scattering measurements, it is anticipated that in this context the number of required CS-based MLFMM computations may be further reduced with adaptive formation of Φ (rather than constituting the N_s excitations randomly, they may be constituted adaptively, with a goal of accelerating CS convergence [13]).

In the CS analysis one must choose a basis or frame Ψ in which to operate, and it is desirable to pick a Ψ for which the signal of interest is sparsely rendered. Although an exhaustive analysis was not performed, for the problem of interest here it was determined that the discrete cosine transform (DCT) yielded better sparseness than a wavelet basis; this is attributed to the fact that often the angle-dependent scattered fields constitute a very smooth function, and therefore the localizing properties of wavelets are less necessary. An area of interest involves an investigation into a Ψ that is best suited for the scattering analysis of interest; in this context Ψ may be complex.

Finally, to simplify the analysis presented here, we considered CS computations at a single frequency, although the basic construct may be extended to estimating the angle *and* frequency dependent properties of the scattered fields. Moreover, many scattering techniques are implemented in the time domain, such as the FDTD method applied in a subset of the examples considered here. It is of interest to examine how the CS formulation may be extended to time domain scattering measurements.

Acknowledgments

The research reported here was supported by DARPA, under the Mathematical Time Reversal (MTR) program, and by ONR, under the Basic Research Challenge program.

References

[1] I. Daubechies, Ten Lectures on Wavelets, SIAM, 1992.
[2] S. Mallat, A Wavelet Tour of Signal Processing, second ed., Academic Press, 1998.
[3] A. Said, W.A. Pearlman, A new fast and efficient image codec based on set partitioning in hierarchical trees, IEEE Trans. Circuits Systems Video Technology 6 (1996) 243–250.
[4] W.A. Pearlman, A. Islam, N. Nagaraj, A. Said, Efficient low-complexity image coding with a set-partitioning embedded block coder, IEEE Trans. Circuits Systems Video Technology 14 (November) (2004) 1219–1235.
[5] W. Pennebaker, J. Mitchell, JPEG: Still Image Data Compression Standard, Springer, New York, NY, 1993.

[6] E. Candès, T. Tao, The Dantzig selector: statistical estimation when p is much larger than n, 2005, preprint.
[7] E. Candès, J. Romberg, T. Tao, Robust uncertainty principles: exact signal reconstruction from highly incomplete frequency information, IEEE Trans. Information Theory 52 (2) (2006) 489–509.
[8] D.L. Donoho, Compressed sensing, IEEE Trans. Information Theory 52 (4) (2006) 1289–1306.
[9] J.A. Tropp, A.C. Gilbert, Signal recovery from partial information via orthogonal matching pursuit, April 2005, preprint.
[10] D.L. Donoho, Y. Tsaig, I. Drori, J.-C. Starck, Sparse solution of underdetermined linear equations by stagewise orthogonal matching pursuit, March 2006, preprint.
[11] Y. Tsaig, D.L. Donoho, Extensions of compressed sensing, Signal Processing 86 (3) (2006) 549–571.
[12] J. Haupt, R. Nowak, Signal reconstruction from noisy random projections, IEEE Trans. Information Theory 52 (9) (2006) 4036–4048.
[13] S. Ji, Y. Xue, L. Carin, Bayesian compressive sensing, IEEE Trans. Signal Processing 56 (6) (2008) 2346–2356.
[14] M. Figueiredo, R.D. Nowak, S.J. Wright, Gradient projection for sparse reconstruction: application to compressed sensing and other inverse problems, 2007, preprint.
[15] R. Harrington, Field Computation by Moment Methods, IEEE Press, 1993.
[16] J. Song, C. Lu, W. Chew, Multilevel fast multipole algorithm for electromagnetic scattering by large complex objects, IEEE Trans. Ant. and Prop. 45 (1997) 1488–1493.
[17] R. Coifman, V. Rokhlin, S. Wandzura, The fast multipole method for the wave equation: a pedestrian prescription, IEEE Ant. and Prop. Magazine 35 (1993) 7–12.
[18] J. He, A. Sullivan, L. Carin, Multilevel fast multipole algorithm for three-dimensional dielectric targets in the vicinity of a lossy half space, Microwave and Optical Technology Letters 29 (2001) 100–104.
[19] E. Candès, T. Tao, Near optimal signal recovery from random projections: universal encoding strategies?, IEEE Trans Information Theory 52 (12) (2006) 5406–5425.
[20] E. Candès, J. Romberg, Sparsity and incoherence in compressive sampling, Inverse Problems 23 (2007) 969–985.
[21] T. Hastie, R. Tibshirani, J. Friedman, The Elements of Statistical Learning, Springer-Verlag, 2001.
[22] E. Candès, J. Romberg, Practical signal recovery from random projections, in: Wavelet Applications in Signal and Image Processing XI, Proc. SPIE Conf. 5914, 2005.
[23] L. Carin, D. Liu, B. Guo, In situ compressive sensing, Inverse Problems 24 (2008).
[24] A. Devaney, A filtered backpropagation algorithm for diffraction tomography, Ultrasonic Imaging 4 (1982) 336–360.
[25] P. Blomberg, G. Papanicolaou, H. Zhao, Super-resolution in time-reversal acoustics, J. Acoust. Soc. of Am. 111 (2002) 230–248.